

1 Three Billion Year Secular Evolution of the Triple Oxygen Isotope Composition of  
2 Marine Chert

3 Justin A. Hayles<sup>a\*</sup>, Laurence Y. Yeung<sup>a</sup>, Martin Homann<sup>b</sup>, Asmita Banerjee<sup>a</sup>, Hehe Jiang<sup>a</sup>, Bing Shen<sup>c</sup>, Cin-Ty Lee<sup>a</sup>

4 <sup>a</sup>Department of Earth, Environmental and Planetary Sciences, Rice University, United States

5 <sup>b</sup> European Institute for Marine Studies, CNRS-UMR6538 Laboratoire Géosciences Océan,  
6 Technopôle Brest-Iroise, Place Nicolas Copernic, 29280 Plouzané, France

7 <sup>c</sup>School of Earth and Space Sciences, Peking University, Beijing, China

8

9 \* Corresponding author: [justin.a.hayles@rice.edu](mailto:justin.a.hayles@rice.edu)

10

11 **Keywords:** Archean, chert, triple-oxygen-isotopes, marine silica

12

13 **Highlights:**

- 14 • Chert samples from the last 3.4 Gyr yield a secular evolution of  $^{18}\text{O}/^{16}\text{O}$  and  $^{17}\text{O}/^{16}\text{O}$
- 15 • Cherts since the Ordovician formed in water with  $^{18}\text{O}/^{16}\text{O}$  and  $^{17}\text{O}/^{16}\text{O}$  close to modern  
16 seawater
- 17 • Precambrian cherts formed in different fluids or in different diagenetic environments
- 18

19  
20 **Abstract:** The  $^{18}\text{O}/^{16}\text{O}$  ratios of ancient marine minerals show a puzzling increase over geologic  
21 time. Long-term changes in temperature, seawater  $^{18}\text{O}/^{16}\text{O}$  ratios, and post-depositional  
22 overprinting can all explain this trend, but few tracers can distinguish between these scenarios.  
23 Here, we report high-precision  $^{18}\text{O}/^{16}\text{O}$  and  $^{17}\text{O}/^{16}\text{O}$  ratios of cherts through 3.4 Ga of Earth's  
24 history. We find that Phanerozoic cherts are consistent with having formed in porewaters that are  
25 isotopically indistinguishable from modern (ice-free) seawater. In contrast, Precambrian cherts  
26 require either formation in waters isotopically distinct from Phanerozoic seawater, or a different  
27 mode of formation. If the early diagenetic formation pathway of Precambrian cherts resembles that  
28 of Phanerozoic cherts, and the Precambrian cherts are unaltered, then the results would imply that  
29 the oxygen-isotope composition of seawater has evolved on billion-year timescales before  
30 reaching its present composition by the Ordovician. Under this interpretation it is estimated that  
31 seawater had  $\delta^{18}\text{O} < -11\text{‰}$  at 3.41 Ga, with surface temperatures  $< 34^\circ\text{C}$ . Although this scenario  
32 provides the simplest explanation for the observed  $^{18}\text{O}/^{16}\text{O}$  trend of marine minerals, other  
33 scenarios which do not require a secular change in seawater  $^{18}\text{O}/^{16}\text{O}$  cannot be ruled out.

34

35

## 36 **1.1 Introduction:**

37         The oxygen isotope composition of seawater is buffered over geologic time by a balance  
38 of high- and low-temperature interactions with the silicate Earth (Gregory and Taylor, 1981;  
39 Muehlenbachs, 1998; Muehlenbachs and Clayton, 1976). These interactions have likely confined  
40 the  $^{18}\text{O}/^{16}\text{O}$  ratio in seawater to within a small range over the Phanerozoic (i.e. linearized notation:  
41  $\delta^{18}\text{O} = \ln[\delta^{18}\text{O}+1] = 0 \pm 2\text{‰}$  relative to VSMOW) (Coogan et al., 2019; Cummins et al., 2014;  
42 Henkes et al., 2018). High-temperature interactions, such as those at seafloor hydrothermal  
43 systems, tend to increase seawater  $\delta^{18}\text{O}$  values, while low-temperature interactions with oceanic  
44 and continental crust tend to lower seawater  $\delta^{18}\text{O}$  values. Yet, details of how this seawater  
45 buffering system operated for early Earth are unknown. The evolution of seawater  $\delta^{18}\text{O}$  may offer  
46 clues to the evolution of the solid Earth over geologic time (Jaffrés et al., 2007; Kasting et al.,  
47 2006). Changing subaerial exposure of mid-ocean ridges, penetration depths of seafloor  
48 hydrothermal circulations, effective seafloor spreading rates, and the spatial extent of volcanic  
49 plateaus can all affect seawater  $\delta^{18}\text{O}$  values by altering the proportions of high- and low-  
50 temperature water-rock interactions at the global scale (Jaffrés et al., 2007; Kamber, 2010; Kasting  
51 et al., 2006).

52         Compilations of data for marine carbonates, phosphates, shales and cherts all show a  
53 secular increase in  $\delta^{18}\text{O}$  values over Earth history (Bindeman et al., 2016; Levin et al., 2014;  
54 Veizer et al., 1997). The oldest minerals show  $\delta^{18}\text{O}$  values that are as much as 15‰ lower than  
55 their modern equivalents. While a secular evolution of seawater  $\delta^{18}\text{O}$  can explain this trend, the  
56 explanation is not unique: the  $\delta^{18}\text{O}$  data are also compatible with scenarios invoking  $\geq 70^\circ\text{C}$  Earth-  
57 surface cooling since the Archean (Knauth and Epstein, 1976; Knauth and Lowe, 2003; Levin et

58 al., 2014; Perry and Lefcariu, 2014) or progressive alteration of marine minerals in meteoric  
59 waters as they age (Levin et al., 2014; Perry and Lefcariu, 2014). This lack of uniqueness has  
60 persisted since the first oxygen-isotope measurements of Archean cherts were reported over 50  
61 years ago (Perry, 1967) because  $\delta^{18}\text{O}$  values alone cannot distinguish between changes in the  
62 isotopic composition of the source water and changes in growth temperature. Clumped-isotope  
63 approaches have emerged as a tool to constrain these quantities independently, but their  
64 compositions in Precambrian carbonates have likely been altered by heating associated with burial  
65 and exhumation (Henkes et al., 2018; Passey and Henkes, 2012; Stolper and Eiler, 2015). Other  
66 approaches have been developed, such as  $\delta^{18}\text{O}$  values in occluded kerogen (Tartèse et al., 2017),  
67 but the degree and nature of alteration in these archives is poorly known. Thus, the idea of a long-  
68 term evolution in seawater  $\delta^{18}\text{O}$  values remains controversial.

69 We hypothesize that  $^{18}\text{O}/^{16}\text{O}$  and  $^{17}\text{O}/^{16}\text{O}$  isotope ratios of cherts—i.e., their triple oxygen-  
70 isotope composition—can constrain the  $\delta^{18}\text{O}$  of ancient porewaters. Ultra-high-precision oxygen  
71 triple-isotope measurements (quantified as  $\Delta^{17}\text{O} = \delta^{17}\text{O} - 0.5305 \times \delta^{18}\text{O}$ ) allow one to probe the  
72  $\delta^{18}\text{O}$ - $\Delta^{17}\text{O}$  relationships between phases, which are bounded by physical-chemical constraints  
73 (Cao and Liu, 2011; Hayles et al., 2018; Hayles et al., 2017). For a given source-water  $\delta^{18}\text{O}$  and  
74  $\Delta^{17}\text{O}$  value, only a bounded range of chert compositions are possible at equilibrium (Hayles et al.,  
75 2018; Sharp et al., 2016; Wostbrock et al., 2018). Similarly, the oxygen triple-isotope composition  
76 of a given chert is only consistent with a narrow set of growth waters. The low permeability and  
77 low oxygen diffusivity in microquartz cherts render them an ideal phase to analyze these variations  
78 because they are resistant to alteration once the crystalline quartz phase has formed (Knauth,  
79 1994): experimental measurements of oxygen diffusion rates in grain boundaries of natural chert

80 samples suggest it would take 30-300 Gyr for exchange to occur across a one-centimeter-thick  
81 layer at 450°C (Farver and Yund, 1991).

82 Earth-system evolution models that predict lower seawater  $\delta^{18}\text{O}$  values early in Earth's  
83 history require a lower ratio of high-temperature to low-temperature water-rock interactions in  
84 Earth's deep past (Jaffrés et al., 2007; Kasting et al., 2006; Wallmann, 2004). An empirically  
85 constrained model for seawater  $\Delta^{17}\text{O}$ , based on the long-term water-rock mass balance formalism  
86 of Muehlenbachs (1998), predicts higher seawater  $\Delta^{17}\text{O}$  values when  $\delta^{18}\text{O}$  values are low (Pack  
87 and Herwartz, 2014; Sengupta and Pack, 2018).

88 To date, triple-oxygen compositions of only one set of Precambrian (2.5 Ga) and  
89 Phanerozoic cherts has been published (Levin et al., 2014). Their compositions show no coherent  
90 pattern, but are generally lower in  $\Delta^{17}\text{O}$  than expected for equilibrium with seawater at a given  
91  $\delta^{18}\text{O}$  value. Closed-system hydrothermal alteration was suggested as a potential driver of triple-  
92 oxygen variability in the rock record, although one Phanerozoic chert (~65 Ma Stevns Klint chert)  
93 was found to be unaltered (Sengupta and Pack, 2018). Given the sparsity of chert triple-oxygen  
94 data, it is not known if the secular evolution in  $\delta^{18}\text{O}$  values is also present in  $\Delta^{17}\text{O}$  values. If the  
95 secular evolution in chert  $\delta^{18}\text{O}$  values is mirrored in their  $\Delta^{17}\text{O}$  values, chert oxygen-isotope  
96 compositions may be diagnostic of changing Earth-system processes through Earth history.

97 In this study, we expanded the record of triple-oxygen isotopes in chert by analyzing the  
98 compositions of suite of marine cherts from the Archaean to late Phanerozoic. Higher  $\Delta^{17}\text{O}$  values  
99 in ancient cherts, together with oxygen triple-isotope compositions that are incompatible with  
100 growth in a modern ice-free ocean, would imply that the  $\delta^{18}\text{O}$  value of diagenetic fluids—and  
101 perhaps seawater—has evolved over Earth history. Chert compositions compatible with growth in  
102 modern-like diagenetic fluids (i.e. seawater) through Earth history would imply robust proportions

103 of global seawater-rock interactions and relatively constant diagenetic environments for marine  
104 chert formation amidst a cooling lithosphere and evolving tectonic boundary conditions.

## 105 **2. Materials and Methods:**

106

### 107 **2.1 Materials**

108

109 Chert samples for this study were taken from units covering 3.4 billion years of Earth's  
110 history from three modern day continents. Samples for this study were taken from the  
111 Monterey/Sisquoc Formation (Miocene) of California, San Andres Limestone (Permian) and  
112 Onate formation (Devonian) of New Mexico, Caballos Novaculite (Devonian) and Ellenberger  
113 Group (Ordovician) of Texas, Liuchapo Formation (Ediacaran) of China, Gunflint Formation  
114 (1.880 Ga) in Ontario and the Frisco Formation (2.521 Ga), Moodies Group (3.22 Ga), Mendon  
115 Formation (3.258 Ga) and Kromberg Formation (3.41 Ga) of South Africa. Specific localities,  
116 references for the samples, GPS coordinates, where known, and some further sample information  
117 can be found in Table S1 in the supplemental. Samples are selected based on purity because the  
118 analytical technique for oxygen isotopes cannot discriminate between the silica component of  
119 chert and detrital components. All samples have been analyzed by LA-ICPMS to verify purity is  
120 greater than 98% SiO<sub>2</sub>, but the results for only a subset of these samples are presented in the  
121 supplemental with the remainder to be presented at a later date.

122

123

### 124 **2.2 Methods**

125 Oxygen isotope analyses were conducted at Rice University using techniques previously  
126 described (Yeung et al., 2018). Prior to oxygen isotope analysis, 2-3 mg chert samples and  
127 silicate standards are loaded onto a sample plate made of 316L steel. The sample plate is then  
128 placed into a cell in the laser fluorination line equipped with a ThF<sub>4</sub> coated ZnSe window. The  
129 cell is evacuated to high vacuum using a turbo pump and an infrared lamp is used to heat the  
130 sample plate through the window. The heating and pumping are continued until the pressure  
131 measured at the pump reads <math>10^{-6}</math> mbar. When all samples are individual grains, this heating step  
132 typically lasts for 3 days, but can take up to a week if hydrous (e.g. opal) or powdered samples  
133 are loaded. At the end of this step, the cell containing the samples is filled with ~30mbar of pure  
134 F<sub>2</sub> gas generated by heating of a potassium fluoronickelate salt (Asprey, 1976). The purity of the  
135 F<sub>2</sub> gas, and in particular the lack of O<sub>2</sub>, is verified using periodic F<sub>2</sub>-only blank tests mimicking  
136 the fluorination procedure but lacking the laser heating step. The samples and standards are  
137 exposed to the fluorine gas atmosphere at room temperature for two days. This prefluorination  
138 step is done to remove any further traces of moisture from the samples but in no instance was an  
139 O<sub>2</sub> yield from this step observed.

140 Oxygen from silica samples and silicate standards are converted to O<sub>2</sub> gas by reaction with  
141 a two-fold excess of purified F<sub>2</sub> gas. Typical operating pressure of F<sub>2</sub> is 60 mbar. Heat for the  
142 reaction is provided by a 10.6 μm CO<sub>2</sub> laser (Synrad 48-2; 25W). Reaction temperatures are  
143 unknown, but the majority of the reaction proceeds above the melting temperature of the silicates  
144 and yields are complete. For all chert samples, no residues remained in the cell after fluorination  
145 indicating the samples were composed of pure silica as most common metal fluorides are solids  
146 under the reaction conditions. The purity of the silica was confirmed for the samples which LA-  
147 ICPMS and electron microprobe analyses were performed (see Supplemental Information). The

148 resulting gas mixture of F<sub>2</sub>, O<sub>2</sub>, SiF<sub>4</sub> and trace impurities (e.g. CF<sub>4</sub>, NF<sub>3</sub>) is first purified  
149 cryogenically at -196°C to remove SiF<sub>4</sub> and any other condensable reaction products (e.g. trace  
150 CF<sub>4</sub>). This is followed by reaction of the F<sub>2</sub> with KBr held at 215°C and condensation of the  
151 products at -196°C. The resulting roughly purified O<sub>2</sub> is collected onto a U-trap filled with silica  
152 gel and forwarded through a 3.05 m × 1/8" OD gas chromatography (GC) column filled with  
153 molecular sieve 5A (80/100 mesh) in a 20 mL/min flow of He carrier gas to remove any trace  
154 NF<sub>3</sub>. Beginning at ~2 minutes after introduction and ending 10 minutes after introduction, the  
155 purified O<sub>2</sub> is recollected in a second silica gel filled U-trap. All processes after the fluorination  
156 reaction are automated in order to reduce user-derived variability therein.

157       The resulting purified O<sub>2</sub> is analyzed for triple oxygen isotope composition on a Nu  
158 Instruments *Perspective IS* mass spectrometer (PS001) equipped with a dual inlet and directly  
159 connected to the fluorination line. Oxygen gas is transferred to the mass spectrometer through a 2  
160 ml silica gel filled transfer tube equipped with an automated LN<sub>2</sub> pump. After collection, the O<sub>2</sub>  
161 is expanded into the sample bellow while the silica gel is heated to 95°C and the bellow is cycled  
162 from 90% to 25% six times over 30 minutes. Similar to the fluorination line operation, sample  
163 transfer to the mass spectrometer is automated to remove user dependencies. Machine analytical  
164 precision for all delta values are 0.002‰ or less. Precision (1σ) for analysis of silica is 0.08‰ for  
165 δ<sup>18</sup>O and 0.004‰ for Δ<sup>17</sup>O based on pooled variance of repeat analyses for silica samples  
166 analyzed to date. Equivalent precisions are attained for UWG-2 (n=7) which is used as a pinning  
167 standard (Valley et al., 1995).

168       Air O<sub>2</sub>, used as a secondary standard for scaling purposes, is purified on a separate GC  
169 column filled with molecular sieve 5A held at -80°C (3.05 m × 1/8" OD; Agilent 7890B GC with  
170 thermal conductivity detector). The outflow of the GC separation is interfaced with the last

171 collection trap of the fluorination line allowing for sample transfer from the fluorination line to  
172 be identical to that for O<sub>2</sub> from silicates.

173 The scale compression correction follows the ‘traditional linear’ scheme of Schoenemann et  
174 al. (2013). Previously, we identified a scale compression in the raw isotope-ratio values from the  
175 mass spectrometer which is significant for triple oxygen isotope measurements and can be  
176 explained fully by a “pressure baseline” (PBL) effect (Yeung et al., 2018). The PBL effect  
177 results from scattering of ions/electrons within the flight tube of the mass spectrometer and is  
178 manifest as a nonzero baseline when the gas is entering the source. Provided that the beam  
179 intensity is fixed based on the major beam ( $m/z=32$ ), the selected scheme approximates the  
180 theoretical correction of the PBL effect to well within analytical uncertainty (Yeung et al., 2018).

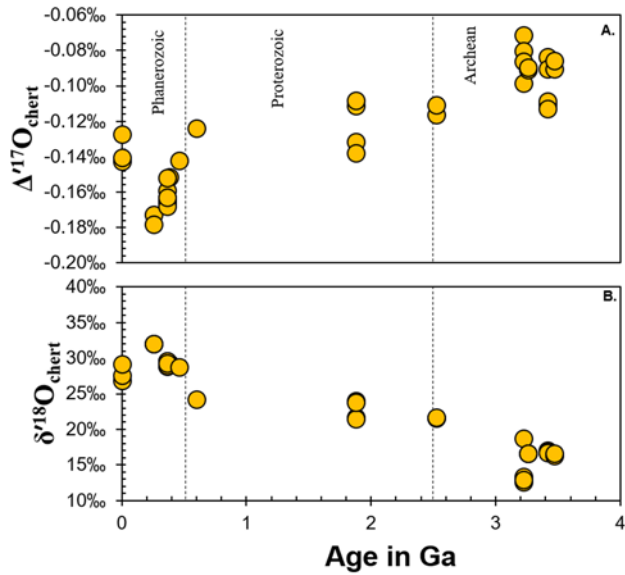
181

182

183 To compare our results directly with the temperature-dependent SiO<sub>2</sub>-water fractionation  
184 calibration of Sharp et al. (2016), we normalize isotope ratios against the UWG-2 standard, which  
185 we assign a  $\Delta^{17}\text{O}$  value of -0.067‰ and a  $\delta^{18}\text{O}$  value of 5.99‰ (Pack and Herwartz, 2014; Sharp  
186 et al., 2016). The measured  $\Delta^{17}\text{O}$  values for UWG-2 and San Carlos Olivine (SCO) differ by ~10  
187 ppm on our setup. This result disagrees with that of (Pack and Herwartz, 2014), which showed  
188 only a 1 ppm difference between these standards. Considering that our SCO sample (SCO99-olv)  
189 may differ from that of other laboratories and that our measured compositions of SCO yield more  
190 variability than our measurements of UWG-2, we use UWG-2 as the primary standard. Further  
191 scaling of the triple-oxygen results is done by assigning a fixed difference in oxygen isotope  
192 compositions between Air-O<sub>2</sub> and UWG-2. The values used are  $\Delta(\delta^{18}\text{O})_{\text{Air} - \text{UWG-2}} = 17.4\text{‰}$ ,  
193 consistent with PBL corrected measurements from our laboratory and  $\Delta(\Delta^{17}\text{O})_{\text{Air} - \text{UWG-2}} = -$

194 0.421‰ which is consistent with previously published values corrected to VSMOW2-SLAP  
195 scaling (Yeung et al., 2018). This scheme yields inter-laboratory agreement in standard materials  
196 within 10 ppm for  $\Delta^{17}\text{O}$  (Yeung et al., 2018).

197  
198 **3. Results:**  
199



200  
201 **Fig. 1.** Oxygen triple-isotope composition of cherts through time. **a.** Measured  $\Delta^{17}\text{O}$  of cherts  
202 analyzed for this study. Point size is plotted to the precision of the measurement ( $0.004\text{‰ } 1\sigma$ ). **b.**  
203 Measured  $\delta^{18}\text{O}(=\ln[\delta^{18}\text{O}+1])$  of cherts analyzed for this study. Uncertainties for  $\delta^{18}\text{O}$  ( $0.08\text{‰}$ )  
204 are smaller than the point size.  
205

**Table 1. Oxygen isotope composition of chert samples and standards.**

<b>Samples</b>	<b>Age (Ga)</b>	<b><math>\delta^{18}\text{O}</math> (‰)</b>	<b><math>\Delta^{17}\text{O}</math> (‰)</b>	<b>n</b>
Monterey/Sisquoc Fm., California USA	0.005	32.435	-0.174	1
	0.005	32.267	-0.163	1
	0.005	27.184	-0.127	1
	0.005	28.011	-0.143	1
	0.005	29.602	-0.141	1
San Andres Limestone, New Mexico, USA	0.275	32.544	-0.176	2
Ocate Fm., New Mexico, USA	0.39	29.726	-0.152	1
Caballos Novaculite, Texas, USA	0.3589	30.045	-0.164	1
	0.3589	29.840	-0.159	1
	0.3589	29.929	-0.166	1
	0.3589	29.366	-0.166	2
	0.3589	29.861	-0.158	2
Ellenberger Gp., Texas, USA	0.46	29.122	-0.142	1
Liuchapo Fm., China	0.6	24.536	-0.124	1
Gunflint Fm., Ontario, Canada	1.88	21.797	-0.110	2
	1.88	24.202	-0.135	2
Frisco Fm., South Africa	2.521	21.826	-0.114	2
Moodies Gp., South Africa	3.22	13.391	-0.071	1
	3.22	12.889	-0.083	2
Mendon Fm., South Africa	3.258	18.880	-0.099	1
	3.258	16.746	-0.090	2
Kromberg Fm., South Africa Black chert (#1) of the BRC	3.416	16.988	-0.087	2
	3.416	17.165	-0.110	1
Kromberg Fm., South Africa White chert of the BRC	3.416	16.906	-0.111	2
	3.416	16.906	-0.111	2
<b>Standards</b>				
San Carlos Olivine		5.603	-0.057	11
UWG-2*		5.972	-0.067	7
Air O <sub>2</sub>		23.222	-0.488	4

\*assigned value discussed in text

†Opal-CT

**Precisions (1 $\sigma$  inter-sample reproducibility) for  $\delta^{18}\text{O}$  are 0.08‰. Precisions for  $\Delta^{17}\text{O}$  are 0.004‰ except for SCO yielding 0.012‰**

209  
210           The cherts show a trend of increasing  $\delta^{18}\text{O}$  and decreasing  $\Delta^{17}\text{O}$  values through time  
211 (Fig.1 and Table 1). The total range in  $\Delta^{17}\text{O}$  values is approximately 0.1‰, with an average  
212 decrease of 0.02‰ per billion years. Phanerozoic marine cherts are characterized by  $\lambda = 0.5223$   
213  $\pm 0.0014$  ( $1\sigma$ ; the slope of a  $\delta^{17}\text{O}$  vs.  $\delta^{18}\text{O}$  cross-plot), and Precambrian cherts by  $\lambda = 0.5263 \pm$   
214  $0.0006$ . These  $\lambda$  values suggest that different processes and/or reservoirs govern oxygen triple-  
215 isotope variations in Phanerozoic and Precambrian cherts. Where repeat analyses were done  
216 (majority of samples; see supplemental) different analyses of the same band or region of the  
217 cherts yields nearly equivalent results, indicating homogeneity of oxygen isotopes in these  
218 samples at spatial scales greater than our sampling scale ( $\sim 1 \text{ mm}^3$ ). Our choice to use the pooled  
219 variance of these analyses for our analytical uncertainty means that any homogeneity at this scale  
220 is factored into our uncertainty ( $\pm 0.004\text{‰}$  for  $\Delta^{17}\text{O}$  and  $\pm 0.08\text{‰}$  for  $\delta^{18}\text{O}$ ).

221

222

223

224

## 225 4. Discussion

226

### 227 4.1 Phanerozoic cherts

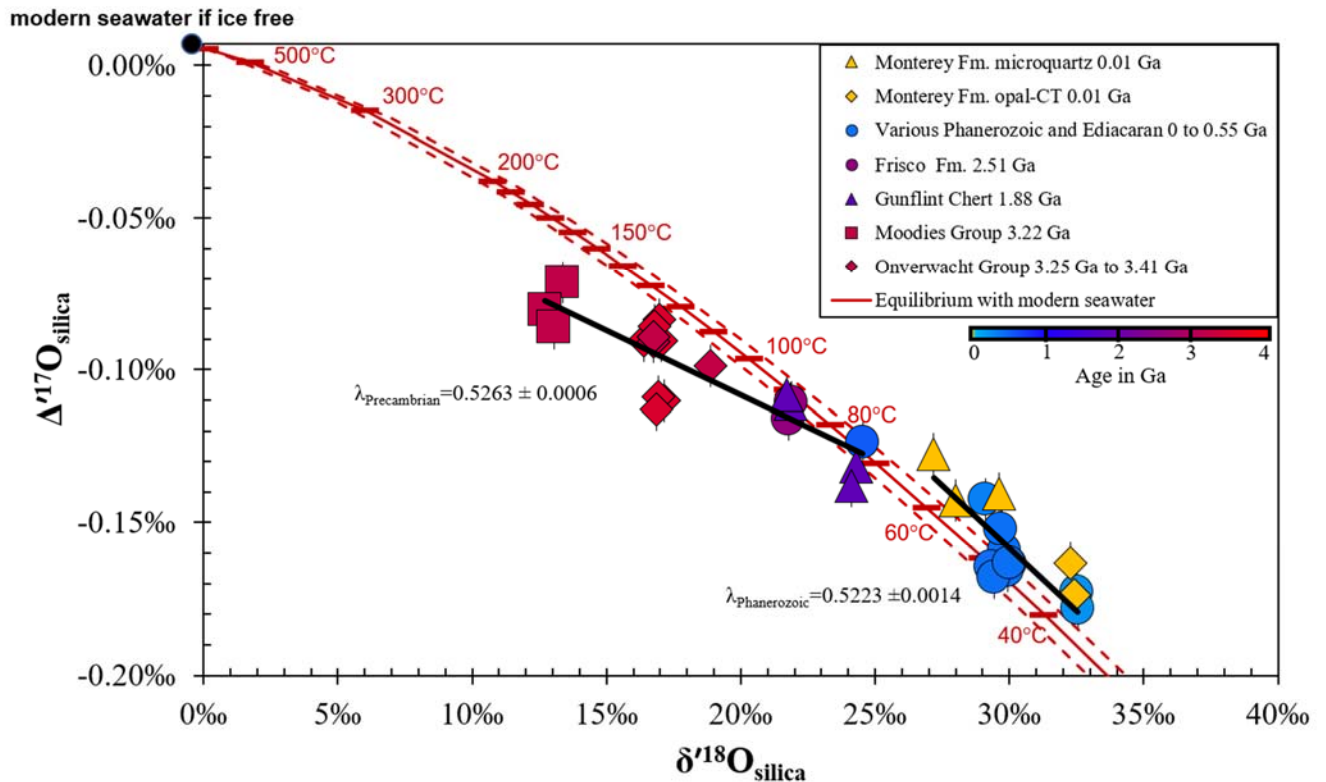


Fig. 2.  $\delta^{18}\text{O}$  vs.  $\Delta^{17}\text{O}$  of cherts and two Neogene Opal-CT samples. Uncertainties are the same as in Fig. 1. The red curve is the range of silica triple-oxygen isotope compositions compatible with formation in the modern ice-free ocean [ $\delta^{18}\text{O} = -1\text{‰}$ ,  $\Delta^{17}\text{O} = 0.0075\text{‰}$  calculated using data in Sharp et al. (2018)] based on the empirical silica-water fractionation estimate of Sharp et al. (Sharp et al., 2016) with slight modification from Wostbrock et al. (2018). Dotted lines around the fractionation curve correspond to compositions of water  $\pm 1\text{‰}$  from a modern ice-free ocean.

228

The oxygen-isotope compositions of chert and opal-CT in the Miocene Monterey

229

Formation (0.01 Ga) are consistent with growth from a water that has a composition offset from

230

a modern (ice-free) ocean by either +1.5‰ in  $\delta^{18}\text{O}$ , +0.008‰ in  $\Delta^{17}\text{O}$ , or some intermediate

231

composition within those bounds (see Fig. 2). This difference could be explained by slight

232 analytical differences between our calibration and that used for the silica-water fractionation  
233 curve (Sharp et al., 2016; Wostbrock et al., 2018). Therefore, the growth waters for these cherts  
234 are isotopically indistinguishable from ice-free modern seawater (hereafter “isotopically  
235 modern” seawater), although a small porewater oxygen-isotope change during chert diagenesis  
236 cannot be ruled out. The Miocene opal and chert compositions are plausibly explained by an  
237 open seawater-porewater system that recrystallizes silica at various temperatures during burial.  
238 This interpretation is consistent with previous work on silica (Murata et al., 1977) and carbonates  
239 (Loyd et al., 2012) in diagenetic settings that showed little evidence for significant porewater  
240  $\delta^{18}\text{O}$  evolution. We thus interpret the  $\lambda$  value of 0.5223 from the Miocene cherts to result from  
241 chert recrystallization in pore waters of constant isotopic composition over a range of  
242 temperatures. For this environment, the diagenetic fluid appears to be a proxy for the isotopic  
243 composition of coeval seawater.

244         Similar to the Miocene cherts, the oxygen-isotope compositions of older Phanerozoic  
245 cherts are consistent with growth from a fluid resembling modern seawater in its oxygen-isotope  
246 composition. Implied growth temperatures based on  $\delta^{18}\text{O}$  in such waters are between  
247 approximately 35°C and 60°C, with a modal temperature of 47°C and no clear correlation  
248 between temperature and age. These conditions, and the range in  $\delta^{18}\text{O}$  and  $\Delta^{17}\text{O}$  values, are  
249 consistent with early diagenetic transformation of low-detritus Opal-A to Opal-CT or  
250 microquartz beneath the seafloor (Keller and Isaacs, 1985). Furthermore, samples identified as  
251 opal-CT from the Monterey Formation (Table S3) yield formation temperatures near 35°C,  
252 which are consistent with the expectation of lower diagenetic temperatures associated with opal-  
253 CT formation (Keller and Isaacs, 1985). This result suggests (1) the isotopic equivalence of  
254 seawater and pore fluids in the environment of chert diagenesis holds through the Phanerozoic

255 and (2) the oxygen isotope composition of seawater has remained roughly constant since at least  
256 the Ordovician. This latter interpretation corroborates recent carbonate clumped-isotope results,  
257 which suggest a seawater  $\delta^{18}\text{O}$  value bound within  $\sim 2\text{‰}$  since the Cambrian (Coogan et al.,  
258 2019; Cummins et al., 2014; Henkes et al., 2018; Ryb and Eiler, 2018).

259         Previously Phanerozoic and Archean cherts were measured by Levin et al. (2014) who  
260 reported  $\Delta^{17}\text{O}$  values relative to UWG-2 measured in their laboratory. Normalizing their chert  
261 results to the UWG-2 composition used here yields mean  $\Delta^{17}\text{O}$  values that are lower than ours  
262 by 0.1‰. The reason for this difference cannot be determined with the information provided in  
263 Levin et al. (2014), although the larger uncertainties in  $\Delta^{17}\text{O}$  standards (e.g.,  $1\sigma = 0.052\text{‰}$  for  
264 UWG-2 and 0.035‰ for NBS-28) suggest that at least some part of the disagreement can be  
265 explained by random error. Potential unquantified triple-oxygen scale compression is difficult to  
266 diagnose in that study given the small  $\delta^{18}\text{O}$  range (4‰) of the standards used. We note that our  
267 reported Phanerozoic chert compositions more closely match marine quartz compositions with  
268 approximately the same  $\delta^{18}\text{O}$  reported in Sharp et al. (2018).

269

## 270 **4.2 Precambrian Cherts**

271         Unlike for the Phanerozoic cherts, the oxygen-isotope compositions of the Latest  
272 Archean and Proterozoic cherts require diagenetic recrystallization at higher temperatures (70-  
273 90°C) and/or in isotopically different waters from those of the Phanerozoic. Paleoarchean cherts  
274 cannot have formed in isotopically modern seawater, invalidating an early hypothesis that they  
275 had grown at elevated temperatures from such fluids (Knauth and Lowe, 2003). Potential  
276 explanations for triple-oxygen compositions of Precambrian cherts involve scenarios in which (i)  
277 the initial growth fluids had a different isotopic composition, (ii) the cherts are internally mixed,

278 i.e., representing multiple generations of silica precipitation that occurred under different  
279 conditions, or (iii) the cherts have been altered after initial deposition. Below, we evaluate these  
280 potential explanations for the isotopic composition of Precambrian cherts, with a focus on those  
281 of the Paleoproterozoic.

282

#### 283 **4.2.1 Scenarios 1 and 2: Early diagenesis in low- $\delta^{18}\text{O}$ , high- $\Delta^{17}\text{O}$ fluids**

284 If the early diagenesis of Phanerozoic cherts is a satisfactory model, i.e., recrystallization  
285 occurred between 35°C and 60°C, then one can estimate the fluid composition required to  
286 precipitate Precambrian cherts in that environment. Using this approach, the oxygen triple-  
287 isotope composition of Onverwacht Group cherts ( $\delta^{18}\text{O} = 17.165\text{‰}$ ,  $\Delta^{17}\text{O} = -0.090\text{‰}$  on  
288 average) imply a diagenetic fluid of  $\delta^{18}\text{O} = -16.4\text{‰}$  to  $-10.7\text{‰}$  and  $\Delta^{17}\text{O} = 0.103\text{‰}$  to  $0.057\text{‰}$   
289 for the Paleoproterozoic. Under this interpretation, younger cherts are compatible with growth in  
290 fluids that were isotopically closer to modern seawater, but those fluids still must have lower  
291  $\delta^{18}\text{O}$  and higher  $\Delta^{17}\text{O}$  values. The origins of these low- $\delta^{18}\text{O}$ , high- $\Delta^{17}\text{O}$  fluids is enigmatic; we  
292 explore the possibility that lighter diagenetic fluids represent (1) meteoric waters and (2) coeval  
293 seawater.

294 The Precambrian cherts can be described by a singular trend different from the  
295 Phanerozoic cherts, with a  $\lambda$  value of 0.5263. This  $\lambda$  value is indistinguishable from that  
296 characterizing meteoric waters with  $\delta^{18}\text{O} > -20\text{‰}$  [ $\lambda = 0.5265 \pm 0.0003$ ; (Sharp et al., 2018)]. A  
297 possible explanation for the compositions of Precambrian cherts is thus subsurface intrusion of  
298 meteoric waters into the early diagenetic environment where they recrystallized. The isotopically  
299 lightest cherts presented here would require nearly pure meteoric waters with low  $\delta^{18}\text{O}$  values  $\leq$   
300  $-11\text{‰}$  if water-to-rock ratios are high. Explaining the temporal trend in triple-oxygen

301 composition using this mechanism requires that meteoric water be a ubiquitous component of  
302 Precambrian chert growth fluids, but insignificant for their Phanerozoic equivalents. If this  
303 interpretation is correct, then the need for this dichotomy in chert formation conditions is further  
304 evidenced by larger compilations of chert  $^{18}\text{O}/^{16}\text{O}$  ratios (Bindeman et al., 2016). Whether a  
305 secular change in chert diagenesis of this nature occurred over Earth history is not known.

306         However, it is clear from studies of the Paleoproterozoic cherts of the Onverwacht Group  
307 (3.41 Ga to 3.25 Ga; plotted as diamonds in Figure 2) and the Buck Reef chert in particular  
308 (BRC; 3.41 Ga), that at least some Paleoproterozoic cherts underwent early diagenetic  
309 recrystallization in an environment similar to that for the Phanerozoic cherts (Knauth and Lowe,  
310 2003). The lines of supporting evidence include: the range of  $\delta^{18}\text{O}$  values matching the  $\sim 7\text{‰}$   
311 range of Phanerozoic cherts (despite lower mean values), the apparent early silicification and  
312 brecciation of “white cherts” of the BRC and Mendon Formation, and silicification prior to the  
313 compaction of carbonaceous particles and relicts of opal-CT lepispheres (Hren et al., 2009;  
314 Knauth and Lowe, 2003; Stefurak et al., 2015; Tice and Lowe, 2006; Trower and Lowe, 2016).  
315 Furthermore, the chert shows no evidence for exogenous inputs from meteoric waters based on  
316  $\delta\text{D}-\delta^{18}\text{O}$  trends, which are more consistent with early diagenesis at temperatures below  $55^\circ\text{C}$   
317 (Hren et al., 2009). The recrystallization fluid for the samples in that study were thus interpreted  
318 to be coeval diagenetic fluids.

319         The samples of BRC analyzed this study were sampled from one of two sections utilized  
320 in the Hren et al. (2009) study, so their geologic context is presumed to apply. If the composition  
321 of the BRC “white” chert is used to solve for the porewater composition—because they are of  
322 higher purity (Table S2), show no textural evidence of secondary silica (Figure S4), and are  
323 believed to have silicified first—then the diagenetic fluid would have  $\delta^{18}\text{O} = -16.6\text{‰}$  to  $-11.0\text{‰}$

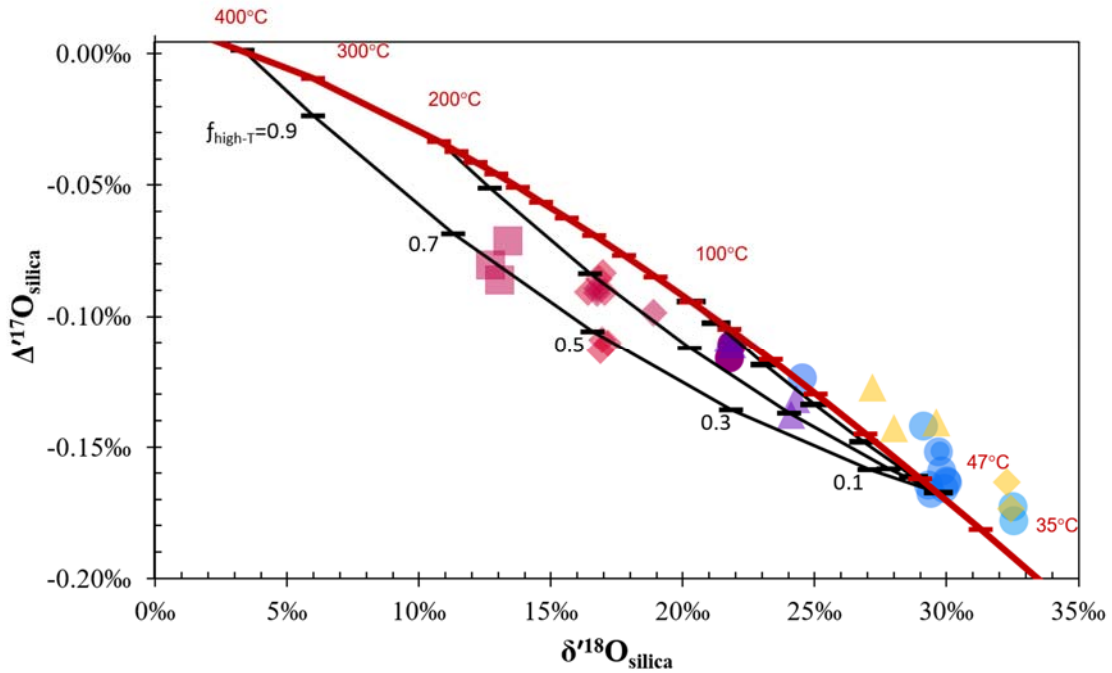
324 and  $\Delta^{17}\text{O} = 0.092\text{‰}$  to  $0.044\text{‰}$ , still different from isotopically modern seawater. Note that the  
325 white chert from the BRC analyzed here has a lower  $\delta^{18}\text{O}$  ( $16.9\text{‰}$ ) than equivalent samples  
326 from the previous study, with a composition closer to the black cherts in the unit. It may indicate  
327 that these particular samples of white chert recrystallized at roughly the same temperature as the  
328 surrounding black chert. In general, the measured cherts from this age have  $\delta^{18}\text{O}$  values at the  
329 low end of those previously measured (Hren et al., 2009; Knauth and Lowe, 2003). Cherts with  
330 these compositions have been previously interpreted as representing the highest-temperature  
331 diagenetic phase.

332         Interestingly, the two 1.88 Ga Gunflint cherts measured here define a triple-oxygen trend  
333 roughly parallel to the trend observed for the Phanerozoic cherts. This parallel trend may imply a  
334 similar diagenetic environment in a fluid of intermediate composition (i.e.,  $\delta^{18}\text{O} \sim -4\text{‰}$ ), but  
335 with the limited data currently available it is not yet possible to determine if this trend is  
336 coincidental. Parallel, triple-isotope trends resembling the Phanerozoic trend within a sequence  
337 would be evidence that the chert oxygen-isotope compositions reflect an early diagenetic  
338 environment similar to Phanerozoic cherts.

339

340

341 **4.2.2 Scenario 3: Mixtures of high- and low-temperature phases**



342

343 *Fig. 3. High and low temperature chert mixture models. The red curve is the range of*  
344 *silica triple-oxygen isotope compositions compatible with formation in modern ice-free*  
345 *seawater). Black lines are two-endmember mixing curves between a higher temperature chert*  
346 *endmember and a lower temperature endmember that were crystallized in porewaters of the*  
347 *same isotope composition. The chert triple oxygen isotope compositions are plotted for*  
348 *comparison.*

349

350 An alternative explanation for the triple-isotope compositions of Precambrian cherts is for  
351 them to be mixtures of silica crystallized at different temperatures. Figure 3 shows two-endmember  
352 mixing curves for high- and low-temperature silica mixtures assuming the pore water composition  
353 in the two environments is equal to isotopically modern seawater. All the Precambrian cherts can  
354 be explained as mixtures of silica crystallized in early diagenetic environments and silica

355 crystallized between 100°C and 400°C. Generally, the Archaean cherts require a higher-  
356 temperature silica mixing endmember than the Proterozoic cherts. The secular trend in oxygen-  
357 isotope compositions would then reflect a cooling of the high-temperature endmember over Earth  
358 history.

359         If the cherts analyzed here are mixtures of high- and low-temperature silica, the  
360 heterogeneity would need to manifest at a scale  $<1 \text{ mm}^3$ , perhaps at the scale of microquartz grains  
361 ( $10^{-5} \text{ mm}^3$ ). Microanalytical techniques may be able to test this hypothesis. A broad distribution in  
362  $\delta^{18}\text{O}$  has been observed in some Precambrian cherts, particularly those of the 1.88 Ga Gunflint  
363 Formation, examples of which were also analyzed here (triangles in Figures 2 and 3). Previous  
364 work indicated an isotopic heterogeneity of  $\sim 12\text{‰}$  at a  $2 \mu\text{m}$  scale in the Gunflint chert, which was  
365 taken as evidence for the presence of a  $\sim 130^\circ\text{C}$  hydrothermal silica mixing endmember (Marin et  
366 al., 2010). Mixing between a high-temperature silica endmember at  $120^\circ\text{C}$  ( $\sim 40\%$ ) and a low-  
367 temperature silica endmember at  $47^\circ\text{C}$  ( $\sim 60\%$ ), both formed in isotopically modern seawater, can  
368 explain the triple-oxygen composition of our Gunflint chert samples. However, this particular  
369 mixture is not unique; there exists a continuum of scenarios for two-endmember (high- and low-  
370 temperature silica) mixtures that can explain these samples if the oxygen-isotope composition of  
371 the growth fluid is allowed to vary. For example, a difference in  $\delta^{18}\text{O}$  of  $12\text{‰}$  can also be attained  
372 if the two end members formed in the same water at temperatures of  $\sim 20^\circ\text{C}$  and  $\sim 70^\circ\text{C}$ , as is  
373 reasonable for the early diagenetic environment. This particular scenario is compatible with water  
374 compositions of  $\delta^{18}\text{O} < -4\text{‰}$  using the bulk oxygen isotope compositions of Gunflint chert  
375 measured here.

376

377

### 378 4.2.3 Scenario 4: Late, closed-system recrystallization of silica

379

380 Finally, we investigate closed-system recrystallization as a possible explanation for the  
381 oxygen-isotope trends in Precambrian cherts. This mechanism was previously considered by  
382 Sengupta and Pack (2018), although our formulation differs slightly in implementation. The  
383 equations for the closed-system water-rock interactions are given by:

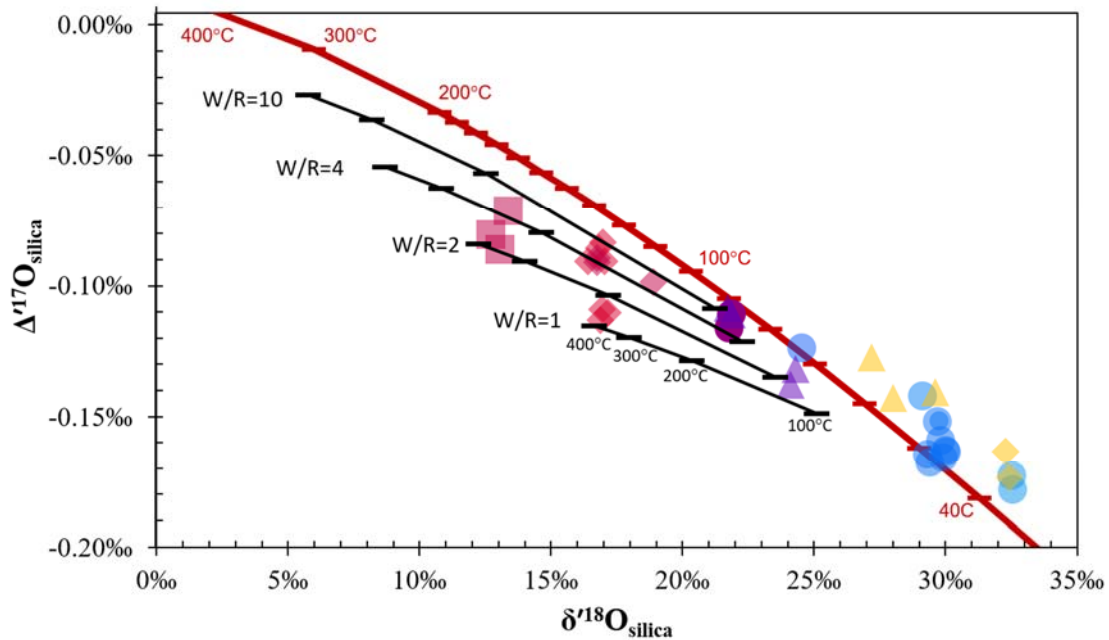
384

385

$$386 \left(\frac{W}{R}\right) R_{w,i} + R_{r,i} = R_{w,f} \left[\alpha + \left(\frac{W}{R}\right)\right] \quad \text{Eq.1}$$

387

388 where  $R$  is the ratio of the heavy isotope to the light isotope, i.e.,  $^{17}\text{O}/^{16}\text{O}$  or  $^{18}\text{O}/^{16}\text{O}$ ,  $\alpha$  is the  
389 temperature dependent fractionation factor for the rock ( $\text{SiO}_2$ ) relative to water, the subscripts  $w$   
390 and  $r$  indicate the parameters for water and rock, respectively, and the subscripts  $i$  and  $f$  indicate  
391 initial and final compositions, respectively.  $W$  and  $R$  are the amounts of oxygen held in water and  
392 the silica phase, respectively.



393

394 *Fig. 4. Closed-system chert recrystallization model results. The red curve is the range of*  
 395 *silica triple-oxygen isotope compositions compatible with formation in modern ice-free*  
 396 *seawater. Black lines give results for closed-system recrystallization at a range of water-rock*  
 397 *ratios (W/R) and temperatures. The chert triple oxygen isotope compositions are plotted for*  
 398 *comparison.*

399

400 We find that for cherts initially formed at 47°C (in modern seawater) and diagenetic fluids  
 401 resembling modern seawater, the secular trend of Precambrian cherts can be explained by closed-  
 402 system recrystallization for  $1 \leq W/R \leq 10$  (see Fig. 4); however, the temperature of alteration must  
 403 undergo a secular decrease through Earth' history. For example, using  $W/R = 4$ , the Onverwacht  
 404 cherts (~3.4 Ga) would be best explained with a closed-system alteration temperature of 175°C,  
 405 while the cherts from the Frisco Formation (2.51 Ga) require a temperature of 110°C. If the

406 diagenetic fluid were meteoric instead, higher water-to-rock ratios are needed to explain the chert  
407 compositions, but secular cooling of those fluids is still required.

408         The need for high water-to-rock ratios argues against the water-rock system being closed  
409 at the grain-scale; for example, if the initial phase consisted of silica granules, as might be implied  
410 by the presence of ripples and cross bedding in the Onverwacht cherts (Tice and Lowe, 2006), then  
411 using a typical porosity of 35%, the bulk W/R ratio is calculated to be  $\sim 0.34$ . Instead, higher water-  
412 to-rock ratios require that the closed system is at the formation scale, perhaps consisting of a  
413 permeable, but unreactive rock that is spatially separated from the samples being analyzed. To  
414 achieve a W/R ratio of 1 using a nominal water-filled porosity of 0.35 would require that 66% of  
415 the rock in the system is unreactive. Higher water-to-rock ratios would require more of the system  
416 to be unreactive, for instance 91% unreactive to reach a W/R of 4. Such a scenario could result  
417 from exchange occurring fastest at the base of a sediment column, where temperatures are highest,  
418 but at a rate slower than the circulation rate of the fluid within the system. In that case, one might  
419 expect distinct closed-system recrystallization trends down-section for different formations in  
420 which permeabilities, porosities, burial rates, and thermal histories differ. In effect, the diagenetic  
421 fluids of these formations would all be different, yielding disparate trajectories in triple-isotope  
422 space. More exhaustive compilations of chert triple-isotope data, once available, will be able to  
423 test this hypothesis.

424

425

### 426 **4.3. Potential implications and relationship to other proxies for ancient temperatures**

427         We will first explore the implications if the BRC samples crystallized in Paleoarchean  
428 diagenetic fluids. Here, we use the interpretation that the BRC represents a diagenetic sequence

429 similar to that of Phanerozoic cherts (Hren et al., 2009; Knauth and Lowe, 2003).  $\delta^{18}\text{O}$  values as  
430 high as 22‰ have been reported in the BRC and interpreted to reflect the lowest-temperature  
431 diagenetic phase in the unit (Knauth and Lowe, 2003). Thus, using  $\delta^{18}\text{O} = -11\text{‰}$  for the diagenetic  
432 fluid and  $\delta^{18}\text{O} = 22\text{‰}$  for the BRC yields a minimum diagenetic temperature of 37°C. This  
433 temperature also serves as an upper limit on seafloor temperatures for this locality during the  
434 Paleoproterozoic. The relatively low temperature is in agreement with the temperature limit (<55°C)  
435 inferred from  $\delta\text{D}-\delta^{18}\text{O}$  pairings (Hren et al., 2009) and the presence of possible diamictites and  
436 gypsum pseudomorphs in lower units of the Onverwacht (de Wit and Furnes, 2016). Moreover, it  
437 is feasible based on recent climate-model predictions (Charnay et al., 2017; Krissansen-Totton et  
438 al., 2018) We note that a minimum diagenetic temperature of 37°C aligns with the lowest  
439 temperature of chert diagenesis we observe in Phanerozoic cherts (~35°C), making this estimate  
440 and interpretation self-consistent.

441

442 The cherts of the Onverwacht Group have been interpreted as marine due to the large lateral  
443 extent of the chert units, the need for large amounts of silica to account for hundreds of meters of  
444 silicified rocks and the presence of evaporites (indicating a saline environment). Thus, interpreting  
445 the chert growth waters as the coeval diagenetic fluid leads naturally to the interpretation that  
446 seawater in the Archean was significantly isotopically lighter. If the diagenetic fluid approximates  
447 coeval seawater for the Precambrian samples—as is case for Phanerozoic cherts—the triple-  
448 isotope data suggest that seawater became progressively more  $^{18}\text{O}$ -enriched over geologic time  
449 (Fig. S1). Any feasible mechanisms for accomplishing a lower  $\delta^{18}\text{O}$  for Paleoproterozoic seawater  
450 require more intense low temperature water-rock interactions and/or less intense high temperature  
451 water-rock interactions earlier in Earth's history (Jaffrés et al., 2007; Kasting et al., 2006; Pack

452 and Herwartz, 2014; Wallmann, 2004). Modeling studies suggest that a seawater  $\delta^{18}\text{O}$  value of -  
453 11‰ can only be achieved by dramatically reducing the proportion of water-rock interactions  
454 occurring at high temperatures (Jaffrés et al., 2007; Kasting et al., 2006). Such a scenario could be  
455 realized if submarine magmatic centers were shallower in the Archean, perhaps associated with  
456 higher mid-ocean ridge crests or more extensive volcanic plateaus (Kamber, 2010; Kasting et al.,  
457 2006; Lambert, 1980). Alternatively, a more sluggish tectonic regime in the Archean (Tang et al.,  
458 2016), characterized by a reduced area of magmatic activity, could lead to a reduction in high-  
459 temperature water-rock chemistry.

460 The Archean seawater composition implied by the early-diagenesis interpretation of  
461 Archean cherts can be compared with estimates obtained from other proxies. The  $\delta^{18}\text{O}$  values in  
462 iron-associated phosphate and kerogen-bound oxygen (Blake et al., 2010; Tartèse et al., 2017) may  
463 first appear to be in disagreement, but the reported uncertainties of those approaches allow them  
464 to be compatible with local surface water having  $\delta^{18}\text{O} \geq -10\text{‰}$  (Chang and Blake, 2015; Tartèse  
465 et al., 2017). Thus, the composition of seawater is not further constrained by these proxies.

466 Sengupta and Pack (2018) recently constructed an empirically constrained seawater triple-  
467 isotope model based on the model of Muehlenbachs (1998). The mass-balance model yields a  $\lambda$   
468 value for seawater evolution of 0.51, which is incompatible with the  $\lambda$  value of 0.526 from  
469 Precambrian cherts in this study if they indeed formed in a fluid resembling Paleoarchean  
470 seawater. Reconciling the geological constraint indicating that the cherts of the Onverwacht Group  
471 in general, and the BRC specifically, represent a diagenetic environment with this study requires  
472 the diagenetic fluids be isotopically depleted relative to coeval seawater. Further constraints can  
473 be provided with additional chert triple oxygen isotope compositions.

474           The other scenarios we consider, i.e. the involvement of meteoric water, late closed system  
475 recrystallization and mixtures between silica formed at high temperature and low temperatures,  
476 imply other secular Earth system trends. In the case of the involvement of meteoric water, a trend  
477 in paleolatitude or paleoaltitude of the source waters would be needed to explain the chert  
478 compositions. Another possible explanation is that of progressive alteration in meteoric waters  
479 over the cherts long history, but this has been argued against in the past (Knauth and Lowe, 2003).  
480 For the other potential explanations, the common trend is the need to invoke a secular change in  
481 the temperature of later alteration. Assuming burial rates are constant, as they would be governed  
482 by surface processes, the simplest explanation is a secular change in the geothermal gradient in the  
483 environment of chert diagenesis. A steeper geothermal gradient in the Archean would bring the  
484 depth with sufficient temperature closer to the surface possibly allowing these cherts to reach the  
485 needed temperatures prior to the loss of their porosity. This may be explained by higher heat  
486 production for the young Earth. Although studies estimating Archean geothermal gradients largely  
487 focus on the gradient at greater depth, geothermal gradients on Archean cratons are thought to be  
488 similar to the modern (Ballard and Pollack, 1988; Lenardic, 1998). It is unclear if near-surface  
489 geothermal gradients should be sufficiently higher in Earth's deep past.

490           Regardless of the interpretation, the presence of a long-term triple-oxygen isotope trend in  
491 Precambrian cherts implies a secular evolution of some boundary condition relevant to chert  
492 diagenesis affecting the isotopic composition of the fluid. Moreover, this evolution appears to have  
493 ceased by the beginning of the Phanerozoic, or has not yet significantly affected Phanerozoic  
494 cherts. Examples of these boundary conditions are the composition of intruding meteoric waters  
495 (e.g. driven by steadily decreasing paleolatitude for the sections), the global-mean temperature of  
496 seawater-rock interactions (i.e. resulting in a change in seawater  $\delta^{18}\text{O}$ ) or the temperature of

497 hypothetical high-temperature alterations (i.e. secular change in the geotherm). These potential  
498 explanations are not exclusive and any combination of them would be consistent with chert oxygen  
499 isotope results. We note that shales, carbonates, and cherts share similar oxygen-isotope trends  
500 through geologic time (Bindeman et al., 2016); our chert  $\Delta^{17}\text{O}$  record resembles that recently  
501 reported for shale, in particular [(Bindeman et al., 2018); see also Fig. S1]. A parsimonious  
502 explanation for the overall trend is the  $\delta^{18}\text{O}$  value of seawater evolved from -11‰ or lower during  
503 the Paleoproterozoic to a modern composition by the Ordovician. However, conflicting geochemical  
504 and modeling evidence in the literature precludes a definitive interpretation at this time (Blake et  
505 al., 2010; Sengupta and Pack, 2018; Tartèse et al., 2017).

506

## 507 **5.1 Conclusions:**

508 The triple-oxygen isotope composition of marine cherts from 3.5 billion years of Earth's  
509 history indicate a switch in some aspect of the factors leading to the oxygen isotope composition  
510 of chert occurring at some time prior to the Ordovician. The oxygen isotope composition of  
511 Phanerozoic cherts reflect recrystallization over a range of early diagenetic temperatures (35°C-  
512 60°C) in a water indistinguishable from that of the modern ocean ( $\delta^{18}\text{O} = 0 \pm 2\text{‰}$ ). Importantly,  
513 the additional constraint provided by  $^{17}\text{O}$  shows that low  $\delta^{18}\text{O}$  values of Archean cherts are  
514 incompatible with a hot (>70°C) surface and an isotopically modern oceans in the Archaean.  
515 Geological and geochemical constraints from the literature implying an early diagenetic origin  
516 for a subset of the measured Archean cherts, when combined with the data presented here,  
517 suggests that at 3.45 Ga diagenetic fluids had a  $\delta^{18}\text{O}$  value of < -11‰, with surface temperatures  
518 <34°C. While this result may be used to indicate a secular evolution or seawater  $\delta^{18}\text{O}$ , alternate

519 feasible explanations for the chert compositions remain which do not require a change in  
520 seawater  $\delta^{18}\text{O}$ .

521

522 **Acknowledgments:** We acknowledge Candace Pettijohn for providing chert samples. We also  
523 acknowledge Tao Sun, Huanting Hu, Boda Li, Jim Kasting and Mark Torres for discussions.

524 **Funding:** Funding for this project was provided by NSF EAR-1806124 to Justin Hayles.

525 Laurence Yeung was partially supported by the David and Lucile Packard Foundation Science  
526 and Engineering Fellowship.

527 **Author contributions:** The manuscript was written by Justin Hayles and Laurence Yeung. Field  
528 work was conducted by Justin Hayles, Asmita Banerjee, Bing Shen and Martin Homann. Oxygen  
529 isotope analysis was conducted by Justin Hayles. LA-ICPMS analysis was conducted by Justin  
530 Hayles and Hehe Jiang. All authors contributed to interpretations.

531

## References

- Asprey, L.B., 1976. The Preparation of Very Pure Fluorine Gas. *Journal of Fluorine Chemistry* 7, 359-361.
- Ballard, S., Pollack, H.N., 1988. Modern and ancient geotherms beneath southern Africa. *Earth and Planetary Science Letters* 88, 132-142.
- Bindeman, I.N., Bekker, A., Zakharov, D.O., 2016. Oxygen isotope perspective on crustal evolution on early Earth: A record of Precambrian shales with emphasis on Paleoproterozoic glaciations and Great Oxygenation Event. *Earth and Planetary Science Letters* 437, 101-113.
- Bindeman, I.N., Zakharov, D.O., Palandri, J., Greber, N.D., Dauphas, N., Retallack, G.J., Hofmann, A., Lackey, J.S., Bekker, A., 2018. Rapid emergence of subaerial landmasses and onset of a modern hydrologic cycle 2.5 billion years ago. *Nature* 557, 545-548.
- Blake, R.E., Chang, S.J., Lepland, A., 2010. Phosphate oxygen isotopic evidence for a temperate and biologically active Archaean ocean. *Nature* 464, 1029.
- Cao, X.B., Liu, Y., 2011. Equilibrium mass-dependent fractionation relationships for triple oxygen isotopes. *Geochimica Et Cosmochimica Acta* 75, 7435-7445.
- Chang, S.J., Blake, R.E., 2015. Precise calibration of equilibrium oxygen isotope fractionations between dissolved phosphate and water from 3 to 37°C. *Geochimica et Cosmochimica Acta* 150, 314-329.
- Charnay, B., Le Hir, G., Fluteau, F., Forget, F., Catling, D.C., 2017. A warm or a cold early Earth? New insights from a 3-D climate-carbon model. *Earth and Planetary Science Letters* 474, 97-109.
- Coogan, L.A., Daëron, M., Gillis, K.M., 2019. Seafloor weathering and the oxygen isotope ratio in seawater: Insight from whole-rock  $\delta^{18}\text{O}$  and carbonate  $\delta^{18}\text{O}$  and  $\Delta 47$  from the Troodos ophiolite. *Earth and Planetary Science Letters* 508, 41-50.
- Cummins, R.C., Finnegan, S., Fike, D.A., Eiler, J.M., Fischer, W.W., 2014. Carbonate clumped isotope constraints on Silurian ocean temperature and seawater  $\delta^{18}\text{O}$ . *Geochimica et Cosmochimica Acta* 140, 241-258.
- de Wit, M.J., Furnes, H., 2016. 3.5-Ga hydrothermal fields and diamictites in the Barberton Greenstone Belt—Paleoarchean crust in cold environments. *Science Advances* 2.
- Farver, J.R., Yund, R.A., 1991. Measurement of oxygen grain boundary diffusion in natural, fine-grained, quartz aggregates. *Geochimica et Cosmochimica Acta* 55, 1597-1607.
- Gregory, R.T., Taylor, H.P., 1981. An oxygen isotope profile in a section of Cretaceous oceanic crust, Samail Ophiolite, Oman: Evidence for  $\delta^{18}\text{O}$  buffering of the oceans by deep (>5 km) seawater-hydrothermal circulation at mid-ocean ridges. *Journal of Geophysical Research: Solid Earth* 86, 2737-2755.
- Hayles, J., Gao, C., Cao, X., Liu, Y., Bao, H., 2018. Theoretical calibration of the triple oxygen isotope thermometer. *Geochimica et Cosmochimica Acta* 235, 237-245.
- Hayles, J.A., Cao, X., Bao, H., 2017. The statistical mechanical basis of the triple isotope fractionation relationship. *Geochemical Perspectives Letters* 3, 1-11.
- Henkes, G.A., Passey, B.H., Grossman, E.L., Shenton, B.J., Yancey, T.E., Pérez-Huerta, A., 2018. Temperature evolution and the oxygen isotope composition of Phanerozoic oceans from carbonate clumped isotope thermometry. *Earth and Planetary Science Letters* 490, 40-50.
- Hren, M.T., Tice, M.M., Chamberlain, C.P., 2009. Oxygen and hydrogen isotope evidence for a temperate climate 3.42 billion years ago. *Nature* 462, 205-208.
- Jaffrés, J.B.D., Shields, G.A., Wallmann, K., 2007. The oxygen isotope evolution of seawater: A critical review of a long-standing controversy and an improved geological water cycle model for the past 3.4 billion years. *Earth-Science Reviews* 83, 83-122.
- Kamber, B.S., 2010. Archean mafic-ultramafic volcanic landmasses and their effect on ocean atmosphere chemistry. *Chem. Geol.* 274, 19-28.

- Kasting, J.F., Howard, M.T., Wallmann, K., Veizer, J., Shields, G., Jaffrés, J., 2006. Paleoclimates, ocean depth, and the oxygen isotopic composition of seawater. *Earth and Planetary Science Letters* 252, 82-93.
- 5 Keller, M.A., Isaacs, C.M., 1985. An evaluation of temperature scales for silica diagenesis in diatomaceous sequences including a new approach based on the Miocene Monterey Formation, California. *Geo-Marine Letters* 5, 31-35.
- Knauth, L.P., 1994. Petrogenesis of chert. *Reviews in Mineralogy and Geochemistry* 29, 233-258.
- Knauth, L.P., Epstein, S., 1976. Hydrogen and oxygen isotope ratios in nodular and bedded cherts. *Geochimica et Cosmochimica Acta* 40, 1095-1108.
- 10 Knauth, L.P., Lowe, D.R., 2003. High Archean climatic temperature inferred from oxygen isotope geochemistry of cherts in the 3.5 Ga Swaziland Supergroup, South Africa. *Geological Society of America Bulletin* 115, 566-580.
- Krissansen-Totton, J., Arney, G.N., Catling, D.C., 2018. Constraining the climate and ocean pH of the early Earth with a geological carbon cycle model. *Proceedings of the National Academy of Sciences*.
- 15 Lambert, R.S.J., 1980. The thermal history of the earth in the Archean. *Precambrian Research* 11, 199-213.
- Lenardic, A., 1998. On the partitioning of mantle heat loss below oceans and continents over time and its relationship to the Archaean paradox. *Geophysical Journal International* 134, 706-720.
- Levin, N.E., Raub, T.D., Dauphas, N., Eiler, J.M., 2014. Triple oxygen isotope variations in sedimentary rocks. *Geochimica Et Cosmochimica Acta* 139, 173-189.
- 20 Loyd, S.J., Corsetti, F.A., Eiler, J.M., Tripathi, A.K., 2012. Determining the Diagenetic Conditions of Concretion Formation: Assessing Temperatures and Pore Waters Using Clumped Isotopes CURRENT RIPPLES. *Journal of Sedimentary Research* 82, 1006-1016.
- Marin, J., Chaussidon, M., Robert, F., 2010. Microscale oxygen isotope variations in 1.9Ga Gunflint cherts: Assessments of diagenesis effects and implications for oceanic paleotemperature reconstructions. *Geochimica et Cosmochimica Acta* 74, 116-130.
- 25 Muehlenbachs, K., 1998. The oxygen isotopic composition of the oceans, sediments and the seafloor. *Chem. Geol.* 145, 263-273.
- Muehlenbachs, K., Clayton, R.N., 1976. Oxygen isotope composition of the oceanic crust and its bearing on seawater. *Journal of Geophysical Research* 81, 4365-4369.
- 30 Murata, K.J., Friedman, I., Gleason, J.D., 1977. Oxygen isotope relations between diagenetic silica minerals in Monterey Shale, Temblor Range, California. *American Journal of Science* 277, 259-272.
- Pack, A., Herwartz, D., 2014. The triple oxygen isotope composition of the Earth mantle and understanding Delta O-17 variations in terrestrial rocks and minerals. *Earth and Planetary Science Letters* 390, 138-145.
- 35 Passey, B.H., Henkes, G.A., 2012. Carbonate clumped isotope bond reordering and geospeedometry. *Earth and Planetary Science Letters* 351-352, 223-236.
- Perry, E.C., 1967. The oxygen isotope chemistry of ancient cherts. *Earth and Planetary Science Letters* 3, 62-66.
- 40 Perry, E.C., Leticariu, L., 2014. 9.5 - Formation and Geochemistry of Precambrian Cherts, in: Holland, H.D., Turekian, K.K. (Eds.), *Treatise on Geochemistry (Second Edition)*. Elsevier, Oxford, pp. 113-139.
- Ryb, U., Eiler, J.M., 2018. Oxygen isotope composition of the Phanerozoic ocean and a possible solution to the dolomite problem. *Proceedings of the National Academy of Sciences* 115, 6602-6607.
- 45 Schoenemann, S.W., Schauer, A.J., Steig, E.J., 2013. Measurement of SLAP2 and GISP  $\delta^{17}\text{O}$  and proposed VSMOW-SLAP normalization for  $\delta^{17}\text{O}$  and  $^{17}\text{O}_{\text{excess}}$ . *Rapid Communications in Mass Spectrometry* 27, 582-590.

- Sengupta, S., Pack, A., 2018. Triple oxygen isotope mass balance for the Earth's oceans with application to Archean cherts. *Chem. Geol.*
- 5 Sharp, Z.D., Gibbons, J.A., Maltsev, O., Atudorei, V., Pack, A., Sengupta, S., Shock, E.L., Knauth, L.P., 2016. A calibration of the triple oxygen isotope fractionation in the SiO<sub>2</sub>–H<sub>2</sub>O system and applications to natural samples. *Geochimica et Cosmochimica Acta* 186, 105-119.
- Sharp, Z.D., Wostbrock, J.A.G., Pack, A., 2018. Mass-dependent triple oxygen isotope variations in terrestrial materials. *Geochemical Perspectives Letters* 7, 27-31.
- Stefurak, E.J.T., Fischer, W.W., Lowe, D.R., 2015. Texture-specific Si isotope variations in Barberton Greenstone Belt cherts record low temperature fractionations in early Archean seawater. *Geochimica et Cosmochimica Acta* 150, 26-52.
- 10 Stolper, D.A., Eiler, J.M., 2015. The kinetics of solid-state isotope-exchange reactions for clumped isotopes: A study of inorganic calcites and apatites from natural and experimental samples.
- Tang, M., Chen, K., Rudnick, R.L., 2016. Archean upper crust transition from mafic to felsic marks the onset of plate tectonics. *Science* 351, 372-375.
- 15 Tartèse, R., Chaussidon, M., Gurenko, A., Delarue, F., Robert, F., 2017. Warm Archean oceans reconstructed from oxygen isotope composition of early-life remnants. *Geochemical Perspectives Letters* 3, 55-65.
- Tice, M.M., Lowe, D.R., 2006. The origin of carbonaceous matter in pre-3.0 Ga greenstone terrains: A review and new evidence from the 3.42 Ga Buck Reef Chert. *Earth-Science Reviews* 76, 259-300.
- 20 Trower, E.J., Lowe, D.R., 2016. Sedimentology of the ~3.3Ga upper Mendon Formation, Barberton Greenstone Belt, South Africa. *Precambrian Research* 281, 473-494.
- Valley, J.W., Kitchen, N., Kohn, M.J., Niendorf, C.R., Spicuzza, M.J., 1995. UWG-2, a garnet standard for oxygen isotope ratios: Strategies for high precision and accuracy with laser heating. *Geochimica Et Cosmochimica Acta* 59, 5223-5231.
- 25 Veizer, J., Bruckschen, P., Pawellek, F., Diener, A., Podlaha, O.G., Carden, G.A.F., Jasper, T., Korte, C., Strauss, H., Azmy, K., Ala, D., 1997. Oxygen isotope evolution of Phanerozoic seawater. *Palaeogeography, Palaeoclimatology, Palaeoecology* 132, 159-172.
- Wallmann, K., 2004. Impact of atmospheric CO<sub>2</sub> and galactic cosmic radiation on Phanerozoic climate change and the marine  $\delta^{18}\text{O}$  record. *Geochemistry, Geophysics, Geosystems* 5, n/a-n/a.
- 30 Wostbrock, J.A.G., Sharp, Z.D., Sanchez-Yanez, C., Reich, M., van den Heuvel, D.B., Benning, L.G., 2018. Calibration and application of silica-water triple oxygen isotope thermometry to geothermal systems in Iceland and Chile. *Geochimica et Cosmochimica Acta* 234, 84-97.
- Yeung, L.Y., Hayles, J.A., Hu, H., Ash, J.L., Sun, T., 2018. Scale distortion from pressure baselines as a source of inaccuracy in triple-isotope measurements. *Rapid Communications in Mass Spectrometry* 0.
- 35

**Acknowledgments:** We acknowledge Candace Pettijohn for providing chert samples. We also acknowledge Tao Sun, Huanting Hu, Boda Li, Patrick Phelps, Jim Kasting and Mark Torres for discussions.

**Funding:** Funding for this project was provided by NSF EAR-1806124 to Justin Hayles. Laurence Yeung was partially supported by the David and Lucile Packard Foundation Science and Engineering Fellowship.

**Author contributions:** The manuscript was written by Justin Hayles and Laurence Yeung. Field work was conducted by Justin Hayles, Asmita Banerjee, Bing Shen and Martin Homann. Oxygen isotope analysis was conducted by Justin Hayles. LA-ICPMS analysis was conducted by Justin Hayles and Hehe Jiang. All authors contributed to interpretations.

**Competing interests:** Authors declare no competing interests.;

**Data and materials availability:** All data is available in the main text or the supplementary materials.